New Journal of Physics
The open access journal at the forefront of physics

Deutsche Physikalische Gesellschaft DPG
IOP Institute of Physics

Published in partnership with: Deutsche Physikalische Gesellschaft and the Institute of Physics

OPEN ACCESS

RECEIVED
4 August 2021

REVISED
14 November 2021

ACCEPTED FOR PUBLICATION
30 November 2021

PUBLISHED
17 December 2021

PAPER

The topological counterparts of non-Hermitian SSH models

Y Z Han, J S Liu and C S Liu*

Hebei Key Laboratory of Microstructural Material Physics, School of Science, Yanshan University, Qinhuangdao, 066004, People's Republic of China

* Author to whom any correspondence should be addressed.

E-mail: csliu@ysu.edu.cn

Keywords: non-Hermitian skin effect, non-Bloch bulk-boundary correspondence, non-Hermitian SSH model, non-Hermitian Aharonov–Bohm effect, topological invariant

Abstract

Inspired by the relevance between the asymmetric coupling amplitude and the imaginary gauge field, we construct the counterpart of the non-Hermitian SSH model. The idea is the nonzero imaginary magnetic flux vanishing when the boundary condition changes from periodic to open. The zero imaginary magnetic flux of the counterpart leads to the eliminating of the non-Hermitian skin effect and the non-Hermitian Aharonov–Bohm effect which ensures the recovery of the conventional bulk-boundary correspondence from the non-Bloch bulk-boundary correspondence. We explain how some the non-Hermitian models can be transformed to the non-Hermitian SSH models and how the non-reciprocal hopping in the non-Hermitian SSH models can be transformed from one term to the other terms by the similarity transformations. We elaborate why the effective imaginary magnetic flux disappears due to the interplay of the non-reciprocal hoppings in the partner of the non-Hermitian SSH model. As the results, we obtain the topological invariants of the non-Hermitian SSH model in analytical form defined in conventional Brillouin zone. The non-Hermitian SSH model in domain configuration on a chain is discussed with this method. The technique gives an alternative way to study the topological properties of non-Hermitian systems.

1. Introduction

The nonconservative phenomena exist widely in natural and artificial systems, e.g. open system coupled to energy or particle sources, or driven by external fields [1–8]. These system can be modelled by the effective non-Hermitian Hamiltonians and exhibit rich exotic characteristics without Hermitian counterparts [9–24]. The prominent character is the breakdown of the usual bulk-boundary correspondence due to the non-Hermitian skin effect [18–20, 25–35]. The non-Hermitian skin effect induces all the bulk states are localized at the boundaries of the system and are indistinguishable from the topological edge states. The pioneering research is the proposal of the generalized Brillouin zone (GBZ) which recovers the correspondence between the winding number based on complex energy with periodic boundaries and the existence of zero modes with open boundaries [25]. Follow this route, the calculation of GBZ becomes an important topic and has drawn extensive attention recently [32, 36, 37].

It is well known that there is a Hermitian counterpart of a non-Hermitian Hamiltonian within the symmetry-unbroken region, in which the two Hamiltonians have an identical real spectrum [38–40]. This allows us to find the nontrivial topological phases of the non-Hermitian Hamiltonian from its Hermitian counterpart. Here, a natural question that arises in this topics is whether there is a partner of non-Hermitian system that share the same topological phase diagrams. As such, the topological invariant of the original model can be obtained from its partner, which can be calculated in an easier way.

In general, the non-Hermitian skin effect comes from the non-reciprocal hoppings of the lattice. The asymmetric couplings are equivalent to an imaginary gauge field applying to the model [10, 33, 41]. Under the periodic boundary condition (PBC), the imaginary gauge field enclosed in an area induces a nonzero imaginary magnetic flux, which is non-Hermitian Aharonov–Bohm (AB) effect as the Hermitian case [33].

The nonzero imaginary magnetic flux breaks the conventional bulk-boundary correspondence. If alternating the non-reciprocal hoppings and obtaining a topological equivalent model which prevents nonzero imaginary magnetic flux, it expects the non-Hermitian skin effect is eliminated in the equivalent model. In particular, its topological properties can be obtain in conventional Brillouin zone and the topological invariants may have the analytical form which is important to understand the whole properties of non-Hermitian system. A similar approach has been applied to the non-Hermitian SSH model without the t_3 term where the bulk states become extended and the bulk topology of the Bloch Hamiltonian predicts the existence of edge states [33].

Motivated by the above considerations, we develop this method to construct the partners of general non-Hermitian SSH models. As shown in the following studies, the central tenet of the construction is first transforming the non-Hermitian effect to the Bloch phase factor with a similarity transformation and then finding the effective imaginary equivalent gauge field. The counterpart of non-Hermitian SSH model is obtained by removing the non-Hermitian AB effect under the open boundary condition (OBC). Although the asymmetry hoppings remain existing in this system, the non-Hermitian is cancelled due to their interplay. The topological invariants based on band-theory are effective to predict the topological nontrivial states.

The remainder of this paper is organized as follows. In section 2, the Hamiltonian of non-Hermitian SSH model and its various equivalent models are presented. We discuss their relationship and show how the non-Hermiticity in SSH models can be transformed from one form to another by the similarity transformations. In subsection 3.1, we show how the effectively gauge field is found and how to construct a partner model of the non-Hermitian SSH model by a similarity transformation. We show the non-Hermitian skin effect is eliminated due to the offset of the imaginary gauge field. Due to the topologically equivalence of the two models, we study the topological phase transitions with the partner models in subsection 3.2. Inspirited by the consistency of the phase transition point with the numerical method, we further apply the non-Hermitian SSH model in domain configuration on a chain in section 4. Finally, a summary and discussion are given in section 5.

2. The non-Hermitian SSH models

The non-Hermitian SSH model is pictorially shown in figure 1(a), and is described by Bloch Hamiltonian $H_k = \psi_k^\dagger h_k \psi_k$ with

$$h_k = d_x\sigma_x + \left(d_y + \mathrm{i}\frac{\gamma}{2}\right)\sigma_y = \begin{pmatrix} 0 & \left(t_1 + \frac{\gamma}{2}\right) + t_2\,\mathrm{e}^{-\mathrm{i}k} + t_3\,\mathrm{e}^{\mathrm{i}k} \\ \left(t_1 - \frac{\gamma}{2}\right) + t_2\,\mathrm{e}^{\mathrm{i}k} + t_3\,\mathrm{e}^{-\mathrm{i}k} & 0 \end{pmatrix}, \tag{1}$$

where $\sigma_x, \sigma_y, \sigma_z$ are the Pauli matrixes for spin-1/2 and $d_x = t_1 + (t_2 + t_3)\cos k$, $d_y = (t_2 - t_3)\sin k$ [42, 43]. The Numb wavefunction is $\psi_k^\dagger = (a_k^\dagger, b_k^\dagger)$. The non-Hermiticity of the Hamiltonian in equation (1) comes from the asymmetric term $t_1 \pm \frac{\gamma}{2}$. By deformation of the graphical non-Hermitian SSH model in figure 1(a), the model can become its equivalent two-leg ladder model in figure 1(b).

There are various equivalent models for this model in equation (1). For example, a mathematically equivalent model is studied in reference [30]. The Hamiltonian is

$$\bar{h}_k = \left(d_x + \mathrm{i}\frac{\gamma}{2}\sin k\right)\sigma_x + \left(d_y + \mathrm{i}\frac{\gamma}{2}\cos k\right)\sigma_y = \begin{pmatrix} 0 & t_1 + t_2\,\mathrm{e}^{-\mathrm{i}k} + \left(t_3 + \frac{\gamma}{2}\right)\mathrm{e}^{\mathrm{i}k} \\ t_1 + t_2\,\mathrm{e}^{\mathrm{i}k} + \left(t_3 + \frac{\gamma}{2}\right)\mathrm{e}^{-\mathrm{i}k} & 0 \end{pmatrix}. \tag{2}$$

This model can be obtained by a similarity transformation under the OBC,

$$\bar{h} = S_1^{-1} h S_1 \tag{3}$$

with a diagonal matrix S_1 whose diagonal elements are judiciously chosen as [25]

$$S_1 = \{1, r_1, r_1, r_1^2, r_1^2, \ldots, r_1^{L/2-1}, r_1^{L/2-1}, r_1^L\}, \tag{4}$$

where $r_1 = \sqrt{\left|\left(t_1 - \gamma/2\right)/\left(t_1 + \gamma/2\right)\right|}$. Under the similarity transformation, the non-Hermiticity in t_1 term is transformed to t_3 term where t_3 term becomes $t_3 r_1^2$ and t_3/r_1^2. The wavefunction $|\psi\rangle = (a_1, b_1, a_2, b_2, \ldots, a_L, b_L)^{\mathrm{T}}$ becomes $|\bar{\psi}\rangle = S_1^{-1}|\psi\rangle$. The intracell hopping becomes $\bar{t}_1 = \sqrt{|t_1^2 - \gamma^2/4|}$ and the t_2 term remains unchanged.

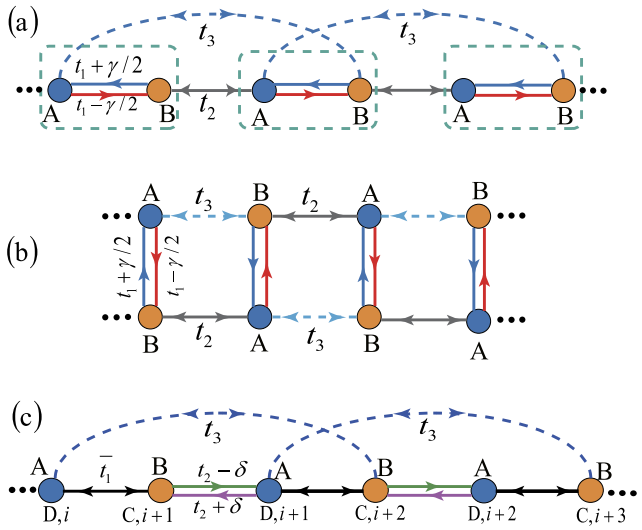

Figure 1. (a) Non-Hermitian SSH model and (b) its equivalent two-leg ladder model. (c) Schematic of the mapping between the non-Hermitian SSH model in equation (1) and the extended non-Hermitian SSH model in equation (6).

Under the OBC, further doing the similarity transformation $\tilde{h} = S_2^{-1}\bar{h}S_2$ with a diagonal matrix

$$S_2 = \mathrm{diag}\{r_2, r_2, r_2^2, r_2^2, \ldots, r_2^{L/2}, r_2^{L/2}\}, \tag{5}$$

the non-Hermiticity in equation (2) is transformed from t_3 term to t_2 term where t_2 term becomes t_2/r_2 and $t_2 r_2$. The wavefunction becomes $|\tilde{\psi}\rangle = S_2^{-1}|\bar{\psi}\rangle$ and the intracell hopping $\bar{t}_1$ remains unchanged when taking $r_2 = r_1^{-2}$. By relabelling the sites A $\to$ D and B $\to$ C and taking $\Delta = t_3$, $t' = \bar{t}_1$, $t - \delta = t_2/r_2$ and $t + \delta = t_2 r_2$ shown in figure 1(c), the Hamiltonian in momentum space takes the form

$$\tilde{H}_k = \sum_k \tilde{\psi}_k^\dagger \tilde{h}_k \tilde{\psi}_k,$$

where $\tilde{\psi}_k = (c_k, d_k)^{\mathrm{T}}$ and

$$\tilde{h}_k = \begin{pmatrix} 0 & t - \delta + t'\,\mathrm{e}^{\mathrm{i}k} + \Delta \mathrm{e}^{-2\mathrm{i}k} \\ t + \delta + t'\,\mathrm{e}^{\mathrm{i}k} + \Delta \mathrm{e}^{2\mathrm{i}k} & 0 \end{pmatrix}. \tag{6}$$

The generalized non-Hermitian SSH model in equation (1) is mapped to the extended non-Hermitian SSH discussed in reference [44].

The non-Hermitian SSH model in equation (2) is also topological equivalence to the model

$$H = \sum_n \Big[\Big(t_1 + \frac{\gamma_1}{2}\Big) c_{n,\mathrm{A}}^\dagger c_{n,\mathrm{B}} + \Big(t_1 - \frac{\gamma_1}{2}\Big) c_{n,\mathrm{B}}^\dagger c_{n,\mathrm{A}} + \Big(t_2 + \frac{\gamma_2}{2}\Big) c_{n,\mathrm{B}}^\dagger c_{n+1,\mathrm{A}} + \Big(t_2 - \frac{\gamma_2}{2}\Big) c_{n+1,\mathrm{A}}^\dagger c_{n,\mathrm{B}} + t_3 \Big(c_{n,\mathrm{A}}^\dagger c_{n+1,\mathrm{B}} + c_{n+1,\mathrm{B}}^\dagger c_{n,\mathrm{A}} \Big) \Big] \tag{7}$$

discussed in reference [27] where $c_{n,\mathrm{A}}^\dagger$ and $c_{n,\mathrm{A}}$ ($c_{n,\mathrm{B}}^\dagger$ and $c_{n,\mathrm{B}}$) are the creation operator and annihilation operator for A (B) site. The non-Hermiticity occurs in t_1 and t_2 terms. One can first do the inverse similarity transformation in equation (5). The non-Hermiticity in t_2 term is transferred to t_3 term. Then further doing the inverse similarity transformation in equation (4), the non-Hermiticity in t_3 term is transferred to t_1 term. After doing the two similarity transformations, the non-Hermiticity in t_2 and t_3 terms disappear and the asymmetric intercell coupling is transformed to symmetrical. The intercell coupling relating to t_1 term remains asymmetrical. After the two-step inverse similarity transformation, the Hamiltonian in equation (7) is transformed to the Hamiltonian in equation (1).

There are various equivalent models for this model in equation (1) in the Hermitian case $\gamma = 0$. For example, when Pauli matrix σ_y is replaced by σ_z and setting $t_1 = M + 4B$, $t_2 + t_3 = 2B$ and $t_2 - t_3 = 2A$, the generalized SSH model h_k can be mapped to 1D Creutz-type model [45]

$$h_k = [M + 4B - 2B\,\cos(k)]\,\sigma_x + 2A\,\sin(k)\,\sigma_z$$

which is the dimensionality reduction BHZ model [46, 47]. Alternatively, when Pauli matrix σ_x is replaced by σ_z and replacing $t_1 = -\mu$, $t_2 + t_3 = -2t$ and $t_2 - t_3 = -2\Delta$, the generalized SSH model h_k can be mapped to 1D Kitaev model [47, 48]

$$h_k = [-2t\ \cos\ k + \mu]\,\sigma_z + 2\Delta\ \sin\,(k)\,\sigma_y.$$

3. The partner model and topological invariant

3.1. The partner model

The asymmetric couplings in t_1 term of equation (1) can be expressed as a symmetric coupling $\bar{t}_1$ with phase factor of amplification/attenuation $e^{\pm\phi}$, i.e. $t_1 \pm \gamma/2 = \bar{t}_1\, e^{\pm\phi}$. Under the basis

$$\psi_k'^{\dagger} = \{a_k^{\dagger}, b_k^{\dagger}\}\begin{pmatrix} e^{-\phi} & 0 \\ 0 & 1 \end{pmatrix} = \{e^{-\phi}a_k^{\dagger}, b_k^{\dagger}\} = \{a_k'^{\dagger}, b_k^{\dagger}\}, \tag{8}$$

the Hamiltonian H_k can be rewritten in the form of

$$H_k = \psi_k'^{\dagger} h_k' \psi_k' = \left[\bar{t}_1 + t_2\, e^{\phi}\, e^{-ik} + t_3\, e^{\phi}\, e^{ik}\right] a_k'^{\dagger} b_k + \left[\bar{t}_1 + t_2\, e^{-\phi}\, e^{ik} + t_3\, e^{-\phi}\, e^{-ik}\right] b_k^{\dagger} a_k'. \tag{9}$$

With the similarity transformation, the asymmetric coupling in equation (8) is transformed from t_1 term to t_2 and t_3 terms shown in figure 2(a). Although the model in equation (1) and the model in equation (9) are topological equivalent, they cannot be considered as the same model due to an extra term $e^{-\phi}$ in $a_k^{\dagger}$. For this reason, the site label A is replaced by A′ which describes that the annihilation operator a of A site is transformed to a'. The AB sublattice becomes A′B sublattice.

Assuming t_1, t_2, t_3 and ϕ to be positive real number, the non-Hermitian skin effect in model (9) can be analysed in real space as follows. When $t_2 \neq 0$ and $t_3 = 0$ shown in figure 2(b), the model (9) is reduced to the general non-Hermitian SSH model. The hopping $t_2\, e^{\phi}$ from B sites to A′ sites is larger than that $t_2\, e^{-\phi}$ from A′ to B sites. The asymmetry hopping causes particles to lean to the right. However, in the case of $t_3 \neq 0$ and $t_2 = 0$ shown in figure 2(c), the model (9) is also reduced to the general non-Hermitian SSH model where the hopping $t_3\, e^{\phi}$ from A′ sites to B sites is larger than that $t_3\, e^{-\phi}$ from B to A′ sites. The asymmetric hopping induces all the eigenstates of the open chain tend to the left boundary. For the case $t_2 = t_3 \neq 0$, the two non-Hermitian skin effects cancel. The Hamiltonian in equation (9) becomes the Hermitian Hamiltonian. Therefore, we conclude that there exists the non-Hermitian skin effect as long as $t_2 \neq t_3$. When $t_2 > t_3$, the non-Hermitian skin effect is governed by the t_2 term and all the states are localized in the right edge. When $t_2 < t_3$, t_3 term dominates the non-Hermitian skin effect which leads to all the states localized in the right edge.

Generally, the amplification and attenuation factors $e^{\pm\phi}$ are equivalent to an imaginary gauge field with the vector potential $i\phi$ applying to the lattice. The effective imaginary gauge field in equation (9) can be analysed in moment space as follows. In the unit cell shown in figure 2(d), two channels (t_2 and t_3) are provided for a particle tunnelling from A′ to B with different hopping amplitude. The two channels lead to a e^{ϕ} phase for a particle tunnelling from A′ site to B site. The product of the above two terms contribute the overall accumulated phase factor $e^{2\phi}$ which suggests the imaginary gauge field with the vector potential be $2(i\phi)$.

The effective imaginary gauge field can also be analysed in real space. Under the PBC, the phase fact $e^{\pm\phi}$ accumulates along the translationally invariant direction. Seen from figures 2(b) and (c), the accumulated factor in one circle is $e^{\pm n\phi}$ for system size $N = 2n$ which is equivalent to an enclosed imaginary magnetic flux $n(i\phi)$ passing through the circle. The total enclosed imaginary magnetic flux is the summation of that from the contribution of t_2 and t_3, which is $2n(i\phi)$. The $2(i\phi)$ enclosed imaginary magnetic flux also suggests the imaginary gauge field with the vector potential be $2(i\phi)$.

We therefore rewrite h_k' in equation (9) as

$$\check{h}_k = \left[\bar{t}_1 + t_2\, e^{-i(k+2i\phi)}\, e^{-\phi} + t_3\, e^{i(k+2i\phi)}\, e^{3\phi}\right]\sigma_+ + \left[\bar{t}_1 + t_2\, e^{i(k+2i\phi)}\, e^{\phi} + t_3\, e^{-i(k+2i\phi)}\, e^{-3\phi}\right]\sigma_-, \tag{10}$$

where $\sigma_{\pm} = \sigma_x \pm i\sigma_y$. Considering the terms $t_2 e^{-i(k+2i\phi)}$ and $t_3 e^{i(k+2i\phi)}$ in equation (10), they are equivalent to an imaginary magnetic field applying to the A′B lattice. As we all know, boundary scattering in the long chain case can still be regarded as a perturbation whether in Hermit case or not. Thus, the Bloch spectra can be well approximated by the bulk spectra, although the OBC breaks the translational symmetry. However, the imaginary magnetic flux vanishes under the OPC. We replace a complex-valued wave vector

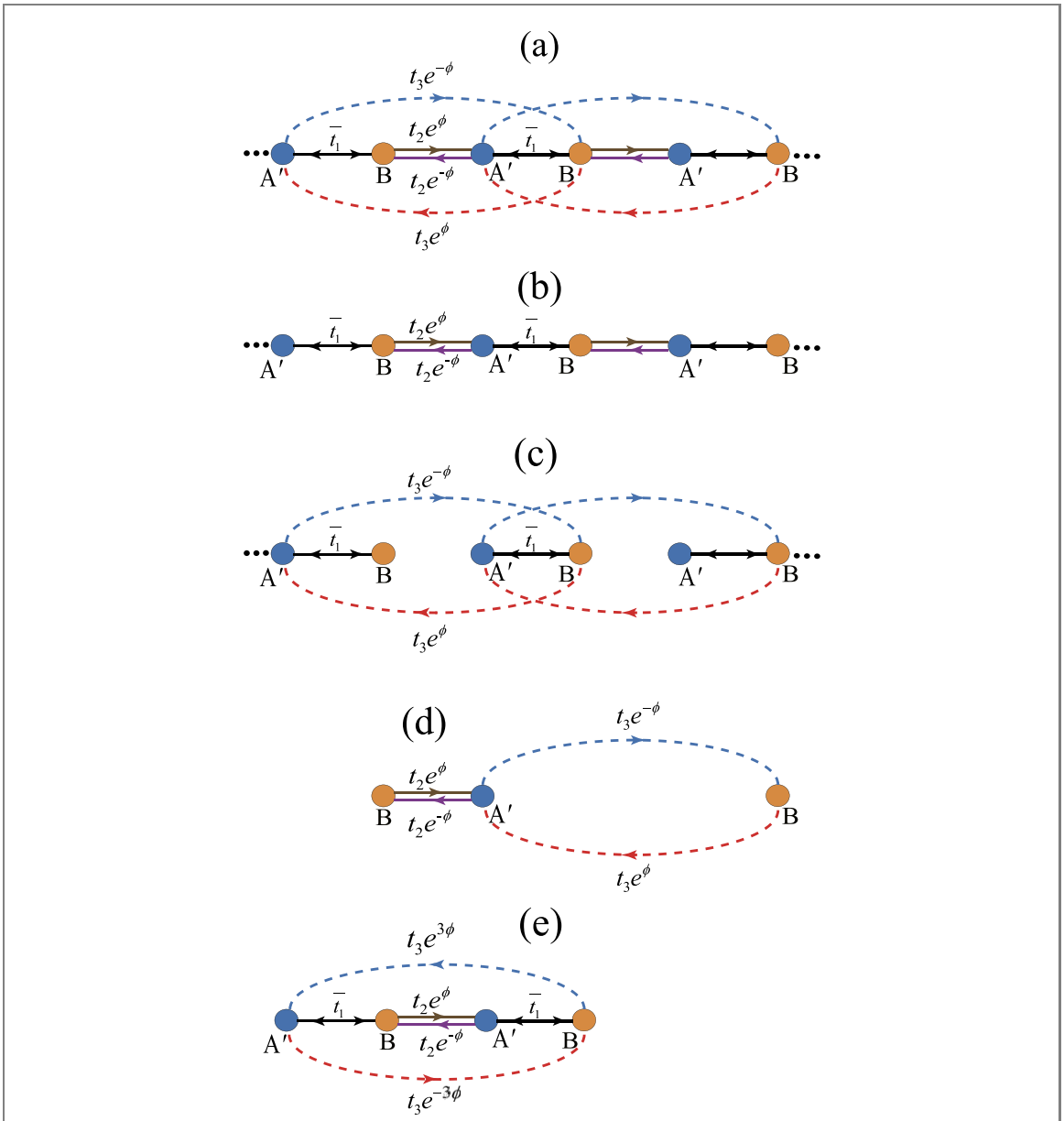

Figure 2. (a) Schematic of the imaginary gauge field in equation (9) when $t_2 \neq 0$ and $t_3 \neq 0$. Illustration of the non-Hermitian skin effect when (b) $t_2 \neq 0$, $t_3 = 0$ and (c) $t_2 = 0$, $t_3 \neq 0$. (d) Illustration of the effective imaginary gauge field in the unity cell of the non-Hermitian SSH model in equation (9). (e) Illustration of the non-Hermitian skin effect cancelling in the unit cell of the partner model in equation (11).

$k + 2\mathrm{i}\phi \to k$ to describe open-boundary spectra. In this replacement, the Hamiltonian (10) can be treated as parameter of k. Accordingly, we define a partner Hamiltonian as follows:

$$\check{h}_k = \check{h}_+(k)\,\mathrm{e}^{\mathrm{i}\theta_+(k)}\sigma_+ + \check{h}_-(k)\,\mathrm{e}^{\mathrm{i}\theta_-(k)}\sigma_-, \tag{11}$$

which is also non-Hermitian Hamiltonian. $\check{h}_+(k)$ and $\theta_+(k)$ are the module and angle of complex function $\bar{t}_1 + t_2\,\mathrm{e}^{-\mathrm{i}k}\,\mathrm{e}^{-\phi} + t_3\,\mathrm{e}^{\mathrm{i}k}\,\mathrm{e}^{3\phi}$. $\check{h}_-(k)$ and $\theta_-(k)$ are the module and angle of complex function $\bar{t}_1 + t_2\,\mathrm{e}^{\mathrm{i}k}\,\mathrm{e}^{\phi} + t_3\,\mathrm{e}^{-\mathrm{i}k}\,\mathrm{e}^{-3\phi}$.

After getting rid of the imaginary gauge field, it is expected that non-Hermitian skin effect disappears concomitantly. The non-existence of non-Hermitian skin effect in equation (11) can be analysed in real space. In the unit cell shown in figure 2(e), $\pm\phi$ in the asymmetry hopping t_2 term is equivalent to an imaginary magnetic field applied to the lattice with an imaginary magnetic vector potential $\mathrm{i}\phi$ along k direction. For the asymmetry hopping t_3 term however, $\pm 3\phi$ can be written as $\pm\phi(3a)$, where the lattice constant $a = 1$. $3a$ indicates three sites have been crossed when a particle hopping from B site to A′ through the t_3 channel. It is also equivalent to an imaginary magnetic field applied to the lattice with an imaginary magnetic vector potential $\mathrm{i}\phi$. However, the imaginary magnetic vector potential is along the $-k$ direction. The two imaginary magnetic vector potentials are cancelled and the imaginary magnetic flux does not exist

under the PBC. No non-Hermitian skin effect occurs in the model (equation (11)), so wave vector k is still a good quantum number which causes the partner model in equation (11) can be discussed in conventional Brillouin zone. Although the partner model in equation (11) is still a non-Hermitian model, the non-Hermitian skin effect disappears due to the interplays of non-Hermitian t_2 and t_3 terms.

The partner model in equation (11) is also effective to the case $t_2 \neq 0$ and $t_3 = 0$. Replacing $k - \mathrm{i}\phi \to k$, the partner model in equation (11) is transformed the standard SSH model with the phase transition point $\bar{t}_1 = t_2$. When $t_3 \neq 0$ and $t_2 = 0$, we can replace $k + 3\mathrm{i}\phi \to k$. The partner model in equation (11) is also transformed the standard SSH model with the phase transition point $\bar{t}_1 = t_3$. The standard SSH model has been studied in references [25, 33].

Under the OBC, the partner Hamilton in equation (11) can also be obtained from the SSH model in equation (1) by a similarity transformation $\check{H} = \check{\Psi}^{\dagger} h \check{\Psi}$ directly with

$$\check{h} = S_3^{-1} h S_3 \quad \text{and} \quad \check{\Psi} = S_3^{-1} \Psi, \tag{12}$$

where $S_3 = S_1 S_2$ is also a diagonal matrix where S_1 and S_2 are given in equations (4) and (5) with $r_1 = r_2 = \mathrm{e}^{\phi}$. The similarity transformation changes the eigen-states without changing its eigen-energy. So the models in equations (1), (9) and (11) are topological equivalent. As shown in subsection 3.2, the topological nontrivial phases can be characterized by the winding number based on the equation (11).

3.2. The topological invariant

According to the usual bulk-boundary-correspondence scenario, the chiral edge states of a 1D open-boundary system should be determined by the winding numbers which are closely related to the Zak phase across the Brillouin zone [49]. For the non-Hermitian system with chiral symmetry and the complex eigenvalues, the winding number of energy is defined as a topological invariant [16, 17, 50]. As $\tilde{k}$ goes across the conventional Brillouin zone, the winding number of energy ν_E is defined as

$$\nu_E = \frac{1}{2\pi} \oint \mathrm{d}k [\partial_k \arg (E_2 - E_1)], \tag{13}$$

where the integral is also taken along a loop with k changing from 0 to 2π. The eigenvalues of Hamiltonian (11) are

$$E_{1,2} = \pm \sqrt{\check{h}_+ (k) \check{h}_- (k)} \exp \left\{ \mathrm{i} \left[\theta_+ (k) + \theta_- (k) \right] / 2 \right\}$$

which are smoothly continuous with k. ν_E is summation of winding numbers of two winding vectors $\check{h}_+ (k) \mathrm{e}^{\mathrm{i}\theta_+(k)}$ and $\check{h}_- (k) \mathrm{e}^{\mathrm{i}\theta_-(k)}$. In Hermitian systems, ν_E is always zero due to the real energy $E_{1,2}$.

The non-Bloch winding number can also be introduced with the 'Q matrix' [20, 25, 30, 51]. The Q matrix is defined by

$$Q(\beta) = |\tilde{u}_{\mathrm{R}}(\beta)\rangle\langle\tilde{u}_{\mathrm{L}}(\beta)| - |u_{\mathrm{R}}(\beta)\rangle\langle u_{\mathrm{L}}(\beta)|,$$

where the right vector $|u_{\mathrm{R}}\rangle$ and left vector $|u_{\mathrm{L}}\rangle$ are defined by

$$\check{h}|u_{\mathrm{R}}\rangle = E(k)|u_{\mathrm{R}}\rangle, \qquad \check{h}^{\dagger}|u_{\mathrm{L}}\rangle = E^*(k)|u_{\mathrm{L}}\rangle.$$

$|\tilde{u}_{\mathrm{R}}\rangle \equiv \sigma_z|u_{\mathrm{R}}\rangle$ and $|\tilde{u}_{\mathrm{L}}\rangle \equiv \sigma_z|u_{\mathrm{L}}\rangle$ are also right and left eigenvectors, with eigenvalues $-E$ and $-E^*$ due to the chiral symmetry. The normalization conditions are $\langle u_{\mathrm{L}}|u_{\mathrm{R}}\rangle = \langle\tilde{u}_{\mathrm{L}}|\tilde{u}_{\mathrm{R}}\rangle = 1$ and $\langle u_{\mathrm{L}}|\tilde{u}_{\mathrm{R}}\rangle = \langle\tilde{u}_{\mathrm{L}}|u_{\mathrm{R}}\rangle = 0$. The Q matrix is off-diagonal, namely $Q = q\sigma_+ + q^{-1}\sigma_-$ where $q = \sqrt{\check{h}_+/\check{h}_-} \exp\{\mathrm{i}[\theta_2 - \theta_1]/2\}$. The non-Bloch winding number is given by

$$\nu_Q = \frac{\mathrm{i}}{2\pi} \int_{C_\beta} q^{-1} \mathrm{d}q \tag{14}$$

which is the difference of two winding numbers of winding vectors $\check{h}_+ (k) \mathrm{e}^{\mathrm{i}\theta_+(k)}$ and $\check{h}_- (k) \mathrm{e}^{\mathrm{i}\theta_-(k)}$.

3.3. Numerical analysis

According to the geometric relations of two winding vectors $\check{h}_+ (k) \mathrm{e}^{\mathrm{i}\theta_+(k)}$ and $\check{h}_- (k) \mathrm{e}^{\mathrm{i}\theta_-(k)}$ in equation (11), at the phase transitions points, the quantums must meet the relationship:

$$\begin{aligned} |\bar{t}_1| &= t_2 \mathrm{e}^{\phi} + t_3 \mathrm{e}^{-3\phi}, \\ |\bar{t}_1| &= t_2 \mathrm{e}^{-\phi} + t_3 \mathrm{e}^{3\phi}. \end{aligned} \tag{15}$$

Taking $t_2 = 1$ and $\gamma = 4/3$ for example, the winding numbers of the two winding vectors in equation (15) with t_1 are shown in figure 3(a). The nontrivial topological phases exist in the regions $|t_1| \leqslant 1.5660$ and $|t_1| \leqslant 1.7050$. Thus, the phase transition points cannot be determined from the equation (15) solely.

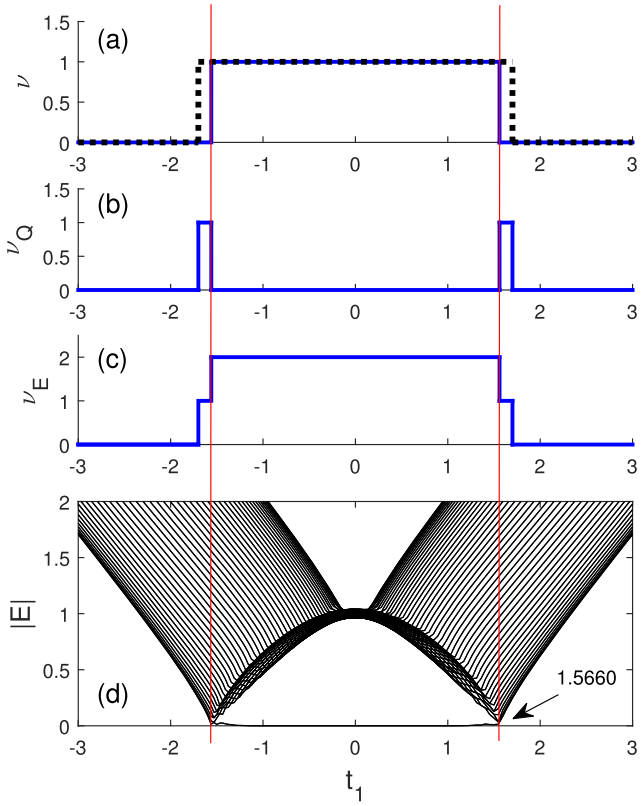

Figure 3. Bulk-edge correspondence with $t_2 = 1$ and $\gamma = 4/3$. The red thin line indicates the topological phase transitions occur at $|t_1| = 1.5660$. (a) The topological invariants (solid line and dotted line) from two different winding vectors in equation (15). (b) The non-Bloch winding number ν_Q which is the difference of the topological numbers in (a). (c) The winding number ν_E of energy which is the summation of the topological numbers in (a). (d) Energy bands in a finite open chain $L = 100$ by diagonalization of equation (11) numerically.

However, the winding numbers ν_E and ν_Q shown in figures 3(b) and (c) show a transition at $|t_1| = 1.5660$. It suggests the topological phase transitions occur at $|t_1| = 1.5660$. The result has been obtained numerically in reference [25] where the GBZ is introduced. We diagonalize the counterpart Hamiltonian in equation (11) numerically to verify the effectiveness of the partner Hamiltonian. The absolute value of eigen-energy $|E|$ as function of t_1 is shown in figure 3(d). The topological transition occurs at $|t_1| = 1.5660$.

To vereigenify the effectiveness of the method, we further analyse the case $t_2 = 1$ and $\gamma = 3/4$. From the winding numbers ν_E and ν_Q of two vectors $h_+(k)\,e^{i\theta_+(k)}$ and $h_-(k)\,e^{i\theta_-(k)}$ in equation (11), the topological transitions occur at $|t_1| = 1.2883$. We diagonalize the Hamiltonians of equivalent model in equation (11) and the original non-Hermitian SSH model in equation (1) numerically under OBC. The open boundary spectra are shown in figures 4(a) and (b). The transition points ($|t_1| = 1.2883$) indicated by red lines confirm the validity of this approach.

Taking $t_1 = 0.6$, an edge state and a bulk state of the equivalent model in equation (11) are plotted in figures 4(d) and (g). The two zero-energy states are all localized in the left boundary. This is due to the breakdown of the inversion symmetry which causes the eigenstates do not have the definite parity. The corresponding edge state and the bulk state of the original non-Hermitian SSH model in equation (1) are plotted in figures 4(e) and (h). Due to the non-Hermitian skin effect, both the edge states and bulk states are localized in the right boundary. To further verify the relationship of the two models given in equation (12), we plot the diagonal element of S_3^{-1} in figure 4(c). Transferring the eigenstates of the original non-Hermitian SSH model in figures 4(e) and (h) with S_3^{-1}, the unnormalized eigenstates of the equivalent model are given in figures 4(f) and (i) which are just the eigenstates in figures 4(d) and (g).

4. An application: the non-Hermitian SSH model in domain configuration on a chain

The defect is an useful tool to probe the nontrivial topological properties of bulk systems [52–55]. Two bulks with topologically distinct phases contacting through a common boundary form a domain wall configuration which is a special topological defect [56–60]. Another type of defect is impurity which can

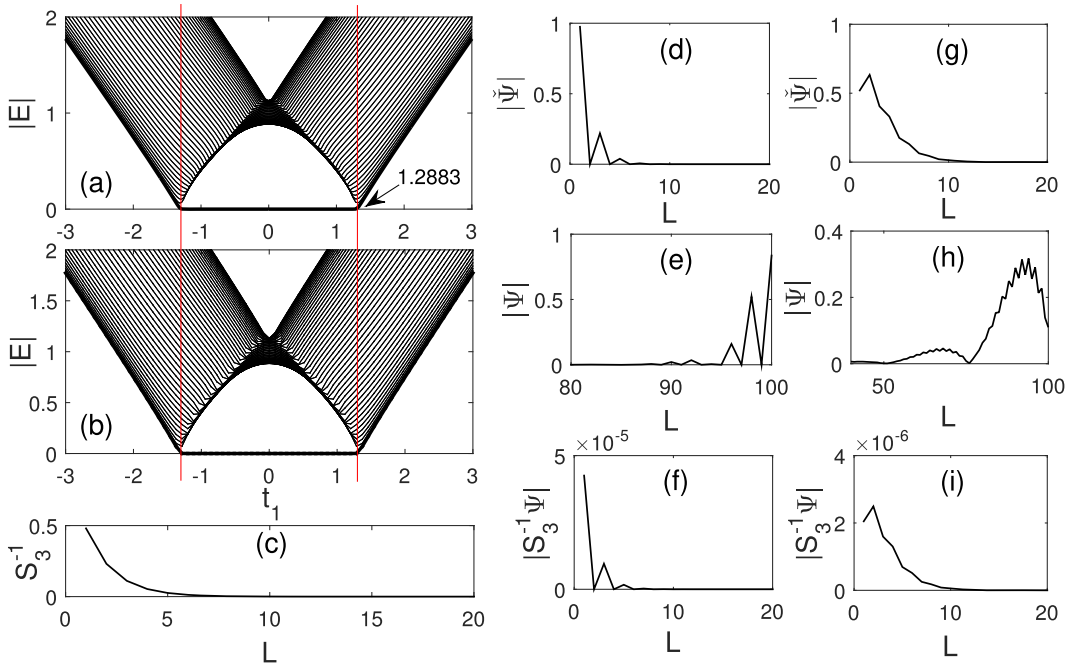

Figure 4. (a) and (b) The open boundary spectra $\check{h}$ in equation (11) and h in equation (1) with $L = 100$, $t_2 = 1$ and $\gamma = 3/4$. The topological transitions occur at $|t_1| = 1.2883$ shown by red thin line. (c) Profile of the diagonal elements of S_3^{-1} in equation (12). (d) and (g) A zero mode and randomly chosen bulk eigenstate $\check{\Psi}$ of equation (11) at $t_1 = 0.6$. (e) and (h) The zero mode and the bulk eigenstate Ψ of equation (1) which are corresponding to the case (d) and (g). (f) and (i) The zero mode and the bulk eigenstate $\check{\Psi}$ of equation (11) is obtained by transforming the wave-functions Ψ in (e) and (h) with the formulae $\check{\Psi} = S_3^{-1}\Psi$.

vary the forward and backward scattering amplitude of the continuous states and induce gap bound states. A hard-wall boundary is a special impurity which is equivalent to the infinity impurity strength and the forward scattering is forbidden. According to the principle of bulk-boundary correspondence, the existence of robust topological states are related to bulk topological invariants. The zero-energy gap states are induced exponentially localized at the defect [61, 62]. In some non-Hermitian topological systems however, the topological boundary modes are determined by non-Bloch topological invariants [25, 32, 36, 37]. In light of recent advances in engineering of the topological defect on non-Hermitian lattices [60, 63, 64], the issue is whether the defect is a useful tool to probe the nontrivial non-Hermitian topological properties.

The nontrivial topological properties of a non-Hermitian SSH model in a domain-wall configuration on a ring have been investigated numerically on GBZ [59]. It finds that both bulk state wave function and the non-Bloch winding numbers of either bulk are dependent on parameters of the other bulk. Motivated by the existence of the counterpart of the non-Hermitian SSH model, the interesting issue is whether the existence of boundary domain states can still be dictated by the two bulk topological invariants of the partner model.

We consider the non-Hermitian SSH model in domain configuration on a chain shown in figure 5. When the length of the two chains is large, the two edges on the chain can be taken as a perturbation. In particular, the coupling of the two edge states can also be neglected in the long chain case. The Hamiltonian can be written as

$$H = H_{\mathrm{L}} + H_{\mathrm{R}} + H_{\mathrm{LR}}, \tag{16}$$

where

$$H_\alpha = \sum_j \left[t_\alpha \, \mathrm{e}^{\phi_\alpha} a_j^\dagger b_j + t_\alpha \, \mathrm{e}^{-\phi_\alpha} b_j^\dagger a_j + t_2 a_{j+1}^\dagger b_j + t_2 b_j^\dagger a_{j+1} \right]$$

and $H_{\mathrm{LR}} = t_2 \left(a_{N_{\mathrm{L}}+1}^\dagger b_{N_{\mathrm{L}}} + b_{N_{\mathrm{L}}}^\dagger a_{N_{\mathrm{L}}+1} \right)$. $\alpha = (\mathrm{L}, \mathrm{R})$ denotes the left or right bulk. $a_j^\dagger$ (a_j) and $b_j^\dagger$ (b_j) are the creation (annihilation) operators for the sublattice sites a and b on the jth unit cell. The left and right bulks have different parameters and contain N_{L} and N_{R} unit cells respectively. The non-Hermicity of the system is from the difference intra-cell hopping $\bar{t}\,\mathrm{e}^{\pm\phi_\alpha} = t_\alpha \pm \gamma/2$. The non-Hermitian SSH model has also chiral symmetry $\Gamma H \Gamma^{-1} = -H$, with the chiral-symmetry operator $\Gamma = \sum_{j=1}^{N_{\mathrm{L}}+N_{\mathrm{R}}} (a_j^\dagger a_j - b_j^\dagger b_j)$.

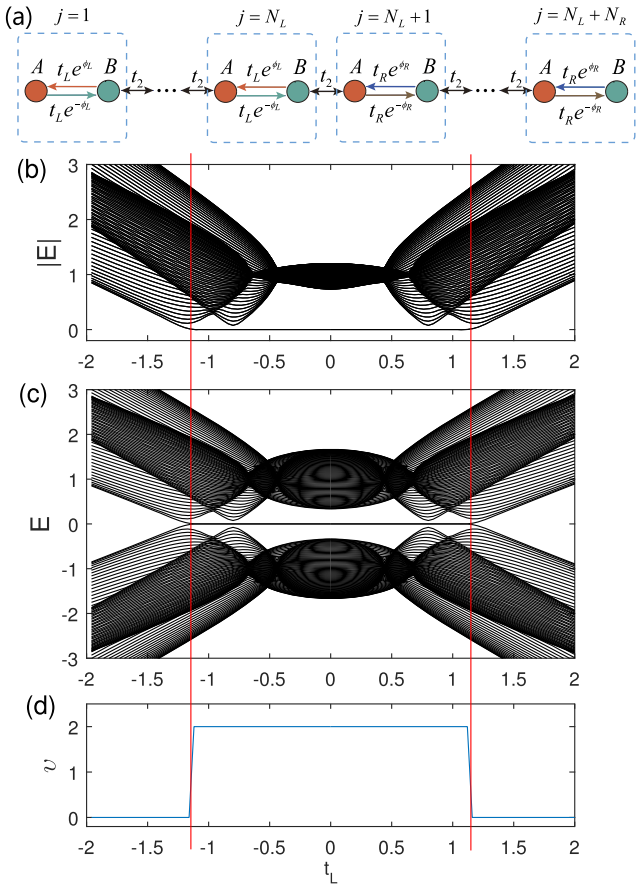

Figure 5. (a) Schematic of a non-Hermitian SSH model under the domain-wall configuration on the chain. The intra-cell hopping from sublattice sites a to b in the left (right) bulk is $e^{-\phi_{L(R)}}$, while the intra-cell hopping from b to a is $t_{L(R)}\, e^{\phi_{L(R)}}$. For simplicity, we assume both bulks have the same t_2. (b) and (c) Show the open boundary spectra E of model (a) and its topological equivalent model as function of t_L. (d) The number of zero-energy of its topological equivalent model as function of t_L. The parameters are taken as $t_2 = 1$, $t_R = 1.5t_2$ and $\gamma = 4t_2/3$. The length of the two chain is $L = 80$. The red vertical lines are used to indicate the topological phase transition at $|t_L| \approx \pm 1.20$.

We do the following transformation to the Hamiltonian in equation (16):

$$H = \langle\Psi|\, h\, |\Psi\rangle = \langle\Phi|\, \bar{h}\, |\Phi\rangle\,,$$

here $\bar{h} = S^{-1}hS$ and

$$|\psi\rangle = (a_1, b_1, \ldots, a_{N_L}, b_{N_L}, \ldots, a_{N_L+N_R}, b_{N_L+N_R})^T$$

and

$$|\Phi\rangle = S|\psi\rangle = (c_1, d_1, \ldots, c_{N_L}, d_{N_L}, \ldots, c_{N_L+N_R}, d_{N_L+N_R})^T.$$

The transformation matrix $S = S_1S_2$. S_1 and S_2 are the diagonal matrices. The diagonal elements of S_1 are set as

$$\left\{1, r, r, r^2, r^2, \ldots, r^{N_L-1}, r^{N_L-1}, r^{N_L}, r^{N_R}, r^{N_R-1}, r^{N_R-1}, \ldots, r^2, r^2, r, r, 1\right\}$$

with $r = e^{(\phi_R-\phi_L)/2}$. After the similarity transformation S_1, we have the same amplification/attenuation $e^{\pm\phi}$ of phase factor in asymmetric couplings of the two bulks, here $\phi = (\phi_R + \phi_L)/2$. Then further doing the similarity transformation S_2 with a diagonal matrix whose diagonal elements are selected as

$$\left(1, r, r, r^2, r^2, \ldots, r^{N_L}, r^{N_L}, \ldots, r^{N_L+N_R-1}, r^{N_L+N_R-1}, r^{N_L+N_R}\right),$$

we get the Hermitian Hamiltonian of the two bulks connecting in a chain configuration

$$\bar{H} = \bar{H}_L + \bar{H}_R + \bar{H}_{LR}, \tag{17}$$

where

$$\bar{H}_\alpha = \sum_j \left(\bar{t}_\alpha c_j^\dagger d_j + t_2 c_{j+1}^\dagger d_j + \mathbf{h.c.}\right)$$

and $\bar{H}_{\rm LR} = t_2\left(c^{\dagger}_{N_{\rm L}+1}d_{N_{\rm L}} + d^{\dagger}_{N_{\rm L}}c_{N_{\rm L}+1}\right)$. The model in equation (17) is topological equivalent to the model in equation (16). The winding number of this model is the difference of winding number $\nu_{\rm R} - \nu_{\rm L}$ of the two bulks. The transition points of the two bulks are $\bar{t}_{\rm L} = \sqrt{t_{\rm L}^2 - \gamma^2/4} = t_2$ and $\bar{t}_{\rm R} = \sqrt{t_{\rm R}^2 - \gamma^2/4} = t_2$.

To verify our analysis, we diagonalize the Hamiltonians in equations (16) and (17) numerically. The open-boundary spectra are shown in figures 5(b) and (c) with the parameters $t_2 = 1$, $t_{\rm R} = 1.5t_2$ and $\gamma = 4t_2/3$. Based on the above analysis, the Hermitian SSH system $\bar{H}_{\rm R}$ in equation (17) is in topological trivial phase due to $\bar{t}_{\rm R}(= 1.34) > t_2$. However, when increasing $|t_{\rm L}|$, the Hermitian SSH system $\bar{H}_{\rm L}$ undergoes the transitions from the topological trivial phase to the topological nontrivial phase. The topological phase transitions occur at $|t_{\rm L}| = \pm\sqrt{t_2^2 + \gamma^2/4} = \pm 1.20$. Shown in figure 5(b), although the open-boundary spectra of equation (16) are complex values, the topological transition occurs at $t_{\rm L} \approx \pm 1.20$ which is consistent with the that from the topological equivalent model in equation (17). We take the zero energy number of the open boundary spectra of topological equivalent model in figure 5(b) as the topological number. Shown in figure 5(d), the topological phase transitions occur at $|t_{\rm L}| = \pm 1.20$. When $|t_{\rm L}| < \pm 1.20$, two topological states appear. One state is localized at the edge of left SSH chain and the other state is localized at the domain of the two chains.

5. Summary

In summary, we have proposed a way to construct a counterpart of the non-Hermitian SSH model to understand the bulk-boundary correspondence of these topological equivalent models. The merit of this method is that the phase transition points are given in analytic form without the numerical calculations in the GBZ. The kernel of this method is finding the effectively imaginary gauge field referring to the non-reciprocal hoppings of the lattice. Under the PBC, it is equivalent to an imaginary magnetic flux passing through the closed chain which induces an imaginary shift of wave-vector or the complex wave-vector. Under the OBC, the imaginary magnetic flux vanishes naturally and the non-Hermitian skin effect is removed accordingly. The corresponding Hamiltonian is the counterpart of the original model and can be discussed in conventional Brillouin zone. The studies indicate that the similarity transformations are important in the constructions. With the similarity transformations, the non-Hermiticity in the SSH model can be shifted from one term to other term. Therefore, some kinds of non-Hermitian lattice models are topological equivalent. We also find that the partner model can be obtained by a similarity transformation under the OBC and the PBC. The method is effective in constructing the counterpart of a class of non-Hermitian model where the non-reciprocal hoppings of the lattice is equivalent to an imaginary magnetic field. However, the method fails to construct the non-Hermitian models in domain configuration on the ring. In view of the complexity of the non-reciprocal hopping, the similarity transformations and the effective imaginary gauge fields may depend on model details. Not all the non-Hermitian models may have the partner models constructed by this method, for example, the models proposed in references [32, 34, 36]. Finding their counterparts is still a challenging subject.

Acknowledgments

This work was supported by Hebei Provincial Natural Science Foundation of China (Grant Nos. A2012203174, A2015203387), Science and Technology Project of Hebei Education Department, China (Grant No. ZD2020200) and National Natural Science Foundation of China (Grant Nos. 10974169, 11304270).

Data availability statement

All data that support the findings of this study are included within the article (and any supplementary files).

ORCID iDs

C S Liu https://orcid.org/0000-0002-5623-3909

References

[1] Rotter I 2009 A non-Hermitian Hamilton operator and the physics of open quantum systems *J. Phys. A: Math. Theor.* **42** 153001
[2] Persson E, Rotter I, Stöckmann H-J and Barth M 2000 Observation of resonance trapping in an open microwave cavity *Phys. Rev. Lett.* **85** 2478–81
[3] Bender C M 2007 Making sense of non-Hermitian Hamiltonians *Rep. Prog. Phys.* **70** 947–1018
[4] Choi Y, Kang S, Lim S, Kim W, Kim J-R, Lee J-H and An K 2010 Quasieigenstate coalescence in an atom-cavity quantum composite *Phys. Rev. Lett.* **104** 153601
[5] Moiseyev N 2011 *Non-Hermitian Quantum Mechanics* (Cambridge: Cambridge University Press)
[6] Reiter F and Sørensen A S 2012 Effective operator formalism for open quantum systems *Phys. Rev.* A **85** 032111
[7] Lu L, Joannopoulos J D and Soljačić M 2014 Topological photonics *Nat. Photon.* **8** 821–9
[8] Rotter I and Bird J P 2015 A review of progress in the physics of open quantum systems: theory and experiment *Rep. Prog. Phys.* **78** 114001
[9] Hatano N and Nelson D R 1997 Vortex pinning and non-Hermitian quantum mechanics *Phys. Rev.* B **56** 8651–73
[10] Hatano N and Nelson D R 1996 Localization transitions in non-Hermitian quantum mechanics *Phys. Rev. Lett.* **77** 570–3
[11] Esaki K, Sato M, Hasebe K and Kohmoto M 2011 Edge states and topological phases in non-Hermitian systems *Phys. Rev.* B **84** 205128
[12] Zhu B, Rong L and Chen S 2014 $\mathcal{PT}$ symmetry in the non-Hermitian Su–Schrieffer–Heeger model with complex boundary potentials *Phys. Rev.* A **89** 062102
[13] Yuce C 2015 Topological phase in a non-Hermitian PT symmetric system *Phys. Lett.* A **379** 1213–8
[14] Lee T E 2016 Anomalous edge state in a non-Hermitian lattice *Phys. Rev. Lett.* **116** 133903
[15] Xu Y, Wang S-T and Duan L-M 2017 Weyl exceptional rings in a three-dimensional dissipative cold atomic gas *Phys. Rev. Lett.* **118** 045701
[16] Leykam D, Bliokh K Y, Huang C, Chong Y D and Nori F 2017 Edge modes, degeneracies, and topological numbers in non-Hermitian systems *Phys. Rev. Lett.* **118** 040401
[17] Shen H, Zhen B and Fu L 2018 Topological band theory for non-Hermitian Hamiltonians *Phys. Rev. Lett.* **120** 146402
[18] Martinez Alvarez V M, Barrios Vargas J E and Foa Torres L E F 2018 Non-Hermitian robust edge states in one dimension: anomalous localization and eigenspace condensation at exceptional points *Phys. Rev.* B **97** 121401
[19] Xiong Y 2018 Why does bulk boundary correspondence fail in some non-Hermitian topological models *J. Phys. Commun.* **2** 035043
[20] Kunst F K, Edvardsson E, Budich J C and Bergholtz E J 2018 Biorthogonal bulk-boundary correspondence in non-Hermitian systems *Phys. Rev. Lett.* **121** 026808
[21] Gong Z, Ashida Y, Kawabata K, Takasan K, Higashikawa S and Ueda M 2018 Topological phases of non-Hermitian systems *Phys. Rev.* X **8** 031079
[22] Liu C-H, Jiang H and Chen S 2019 Topological classification of non-Hermitian systems with reflection symmetry *Phys. Rev.* B **99** 125103
[23] Kawabata K, Shiozaki K, Ueda M and Sato M 2019 Symmetry and topology in non-Hermitian physics *Phys. Rev.* X **9** 041015
[24] Kawabata K, Bessho T and Sato M 2019 Classification of exceptional points and non-Hermitian topological semimetals *Phys. Rev. Lett.* **123** 066405
[25] Yao S and Wang Z 2018 Edge states and topological invariants of non-Hermitian systems *Phys. Rev. Lett.* **121** 086803
[26] Yao S, Song F and Wang Z 2018 Non-Hermitian Chern bands *Phys. Rev. Lett.* **121** 136802
[27] Yokomizo K and Murakami S 2019 Non-Bloch band theory of non-Hermitian systems *Phys. Rev. Lett.* **123** 066404
[28] Song F, Yao S and Wang Z 2019 Non-Hermitian skin effect and chiral damping in open quantum systems *Phys. Rev. Lett.* **123** 170401
[29] Lee C H and Thomale R 2019 Anatomy of skin modes and topology in non-Hermitian systems *Phys. Rev.* B **99** 201103
[30] Song F, Yao S and Wang Z 2019 Non-Hermitian topological invariants in real space *Phys. Rev. Lett.* **123** 246801
[31] Borgnia D S, Kruchkov A J and Slager R-J 2020 Non-Hermitian boundary modes and topology *Phys. Rev. Lett.* **124** 056802
[32] Zhang K, Yang Z and Fang C 2020 Correspondence between winding numbers and skin modes in non-Hermitian systems *Phys. Rev. Lett.* **125** 126402
[33] Jin L and Song Z 2019 Bulk-boundary correspondence in a non-Hermitian system in one dimension with chiral inversion symmetry *Phys. Rev.* B **99** 081103
[34] Zeng Q-B, Yang Y-B and Xu Y 2020 Topological phases in non-Hermitian Aubry–André–Harper models *Phys. Rev.* B **101** 020201
[35] Lee C H, Li L, Thomale R and Gong J 2020 Unraveling non-Hermitian pumping: emergent spectral singularities and anomalous responses *Phys. Rev.* B **102** 085151
[36] Yi Y and Yang Z 2020 Non-Hermitian skin modes induced by on-site dissipations and chiral tunneling effect *Phys. Rev. Lett.* **125** 186802
[37] Yang Z, Zhang K, Fang C and Hu J 2020 Non-Hermitian bulk-boundary correspondence and auxiliary generalized Brillouin zone theory *Phys. Rev. Lett.* **125** 226402
[38] Bender C M and Boettcher S 1998 Real spectra in non-Hermitian Hamiltonians having PT symmetry *Phys. Rev. Lett.* **80** 5243–6
[39] Ali M 2002 Pseudo-Hermiticity versus PT symmetry: the necessary condition for the reality of the spectrum of a non-Hermitian Hamiltonian *J. Math. Phys.* **43** 205–14
[40] Li C, Zhang X Z, Zhang G and Song Z 2018 Topological phases in a Kitaev chain with imbalanced pairing *Phys. Rev.* B **97** 115436
[41] Longhi S 2017 Nonadiabatic robust excitation transfer assisted by an imaginary gauge field *Phys. Rev.* A **95** 062122
[42] Su W P, Schrieffer J R and Heeger A J 1979 Solitons in polyacetylene *Phys. Rev. Lett.* **42** 1698–701
[43] Wu H C, Yang X M, Jin L and Song Z 2020 Untying links through anti-parity-time-symmetric coupling *Phys. Rev.* B **102** 161101
[44] Yin C, Jiang H, Li L, Rong L and Chen S 2018 Geometrical meaning of winding number and its characterization of topological phases in one-dimensional chiral non-Hermitian systems *Phys. Rev.* A **97** 052115
[45] Creutz M 1999 End states, ladder compounds, and domain-wall fermions *Phys. Rev. Lett.* **83** 2636–9

[46] Bernevig B A, Hughes T L and Zhang S-C 2006 Quantum spin Hall effect and topological phase transition in HgTe quantum wells *Science* **314** 1757–61
[47] Guo H-M 2016 A brief review on one-dimensional topological insulators and superconductors *Sci. China Phys. Mech. Astron.* **59** 637401
[48] Kitaev A Y 2001 Unpaired Majorana fermions in quantum wires *Phys. Usp.* **44** 131–6
[49] Zak J 1989 Berry's phase for energy bands in solids *Phys. Rev. Lett.* **62** 2747–50
[50] Jiang H, Yang C and Chen S 2018 Topological invariants and phase diagrams for one-dimensional two-band non-Hermitian systems without chiral symmetry *Phys. Rev.* A **98** 052116
[51] Chiu C-K, Jeffrey C, Teo J C Y, Schnyder A P and Ryu S 2016 Classification of topological quantum matter with symmetries *Rev. Mod. Phys.* **88** 035005
[52] Teo J C Y and Kane C L 2010 Topological defects and gapless modes in insulators and superconductors *Phys. Rev.* B **82** 115120
[53] Kimme L and Hyart T 2016 Existence of zero-energy impurity states in different classes of topological insulators and superconductors and their relation to topological phase transitions *Phys. Rev.* B **93** 035134
[54] Lu J, Shan W-Y, Lu H-Z and Shen S-Q 2011 Non-magnetic impurities and in-gap bound states in topological insulators *New J. Phys.* **13** 103016
[55] Lang L-J and Chen S 2014 Topologically protected mid-gap states induced by impurity in one-dimensional superlattices *J. Phys. B: At. Mol. Opt. Phys.* **47** 065302
[56] Malzard S, Poli C and Schomerus H 2015 Topologically protected defect states in open photonic systems with non-Hermitian charge-conjugation and parity-time symmetry *Phys. Rev. Lett.* **115** 200402
[57] Xiao L, Deng T, Wang K, Zhu G, Wang Z, Yi W and Xue P 2020 Non-Hermitian bulk-boundary correspondence in quantum dynamics *Nat. Phys.* **16** 761–6
[58] Helbig T *et al* 2020 Generalized bulk-boundary correspondence in non-Hermitian topolectrical circuits *Nat. Phys.* **16** 747–50
[59] Deng T-S and Yi W 2019 Non-Bloch topological invariants in a non-Hermitian domain wall system *Phys. Rev.* B **100** 035102
[60] Lang L-J, Wang Y, Wang H and Chong Y D 2018 Effects of non-Hermiticity on Su–Schrieffer–Heeger defect states *Phys. Rev.* B **98** 094307
[61] Schomerus H 2013 Topologically protected midgap states in complex photonic lattices *Opt. Lett.* **38** 1912–4
[62] Longhi S 2014 Bound states in the continuum in PT-symmetric optical lattices *Opt. Lett.* **39** 1697–700
[63] Yuce C 2018 Edge states at the interface of non-Hermitian systems *Phys. Rev.* A **97** 042118
[64] Wu Y-J and Hou J 2019 Symmetry-protected localized states at defects in non-Hermitian systems *Phys. Rev.* A **99** 062107